Progress In Electromagnetics Research C, Vol. 18, 87–101, 2011

INDUCTIVE TRI-BAND DOUBLE ELEMENT FSS FOR SPACE APPLICATIONS

D. Ramaccia and A. Toscano

Department of Applied Electronics
University of Rome RomaTre
Via della Vasca Navale 84, Rome 00146, Italy

A. Colasante, G. Bellaveglia, and R. Lo Forti

TeS — Teleinformatica e Sistemi
Via Tor Tre Teste 229, Roma 00155, Italy

Abstract—In this contribution we propose the design of an inductive Frequency Selective Surface (FSS) with double resonant elements aimed at the achievement of a simple well-performing, dielectric-free, space filter screen able to separate the Ku band from the Ka band. The FSS performance is compared to that of a typical double ring FSS which major drawback is the use of a dielectric substrate that leads to unavoidable additional transmission losses and makes the dichroic mirror more complex with respect to a simple single perforated screen. For all applications in which the FSS is asked to be as simple as possible and the transmission losses specifications are severe, the Inductive FSS Double Resonant Elements here proposed turns out to be an interesting alternative to typical Double Ring FSS.

1. INTRODUCTION

Frequency Selective Surfaces (FSS) are object of continuous research because of their the spatial filtering capability of electromagnetic waves. They have been used in many applications, such as antenna radomes, electromagnetic filtering devices, multi-band antennas, wireless security and satellites [1–3].

Received 5 October 2010, Accepted 26 November 2010, Scheduled 3 November 2010
Corresponding author: Davide Ramaccia (davide.ramaccia@gmail.com).

In principle, according to the FSS theory, more than one solution might be found depending on the type of FSS (Inductive or Capacitive), type of single-cell element (crossed-dipoles, dual-rings, etcetera) and FSS metal depth. All these solutions might offer strength points as well as weak points and a well-performing FSS is not easy to design. Though one or more layered Capacitive FSS with double or multi ring elements already exist as a solution for the multi-band FSS (see [4, 5]), inductive FSS (based on metallic perforated screens) would be in general preferable, especially when thinking of a mass market application, because of the huge reduction of costs with respect to all FSS structures that use dielectric substrates.

In this paper, three possible solutions have been shown before arriving to the final design. The first (Design 1) involves an inductive Double Ring FSS plate with no use of dielectric substrate (ideally floating patch elements), the second (Design 2) is a scaled version of the first using a dielectric substrate as support (just to make the first design feasible). The third one (Design 3) is finally an inductive FSS based on a simple metallic plate with circular holes on a square grid. The latter turned out to be much cheaper but not performing well in all bands. Finally, we present a Dual Element FSS Design solution which improves the performance of Design 3 keeping all the advantages of single element perforated screen.

In all analyses it is assumed that the incident field is a perfect uniform plane-wave impinging the plate by an angle of 0 degrees with respect to the normal. All FSS plates are supposed to be flat and infinitely extended. The optimized FSS was expected to be reflective at the Ku band and transparent at two Ka sub-bands (20 and 30 GHz for RX and TX respectively). All analyses have been carried out using the last available version of *CST Microwave Studio*®.

2. PROJECT SPECIFICATIONS

Let us imagine the FSS designer to face with a problem in which FSS is supposed to be reflective at Ku RX-band and transparent at the Ka-Bands (Both RX and TX).

Electrical design specifications for the dichroic mirrors are generally the result of a more complete high level loss-budget analysis which also takes into account for the other devices of the system (such as Ku band receivers). For simplicity, let us make the assumption that a transmission/reflection loss of about -0.5 dB is acceptable in the three bands (see Table 1).

Table 1. Project specifications.

Bands	Frequencies	Value
Ku RX Band	$f = [10.7, 12.75]\,\text{GHz}$	$S_{21} \leq -10\,\text{dB}$
Ka RX Band	$f = [19.7, 20.2]\,\text{GHz}$	$S_{21} \geq -0.5\,\text{dB}$
Ka TX Band	$f = [29.5, 30.0]\,\text{GHz}$	$S_{21} \geq -0.5\,\text{dB}$

3. TRADITIONAL FSS CONFIGURATIONS

3.1. Double Ring FSS

For more than ten years, dichroic plates designed to multiplex the S, X, Ku and Ka frequency bands used to employ Double-Ring FSS [4, 5] or two concentric square loops [6, 7]. The choice of concentric ring elements is based on the fact that the ring's geometry is particularly conformable to the circular polarization requirement. Following the work of Munk [1, 2], there exists one resonant frequency for the free-standing single ring and this frequency, f_R, is approximately given by:

$$2\pi R = \lambda_0 = \frac{c}{f_R} \tag{1}$$

where $R = R_{in}$, R_{out}, λ_0 the wavelength at the frequency with maximum transmission, f_R the resonance frequency of the element and c the speed of light in vacuum. When the number is increased from one to two-concentric rings (Fig. 1), there will be two different resonant frequencies. When the FSS structure is composed by metallic rings on a dielectric substrate (capacitive FSS), the incident electromagnetic wave is reflected at the resonant frequency. On the contrary, when the FSS structure is composed by a metallic screen with perforated rings (inductive FSS), the incident electromagnetic wave is transmitted at the resonant frequency. The latter is considered and shown in Fig. 1.

The calculated transmission coefficients S_{21} versus frequency are shown in Fig. 2. Key values of S_{21} in the frequency regions of interest and for both polarizations are listed in Table 3. The performance results are quite good for both Ku and Ka bands.

The response for TE and TM excitations are identical, as expected for a symmetrical element (in this case, circular rings). In Table 3, the worst computed transmission coefficient S_{21} in the bands of interest are listed in order to compare it with the specification in Table 1. On the contrary Table 4 lists the range of frequencies in which the $S_{21} \geq -0.5\,\text{dB}$. It is so observed that the frequency sub-bands in which the transmission curve has acceptable values are actually wider than those required in the specs (Table 1).

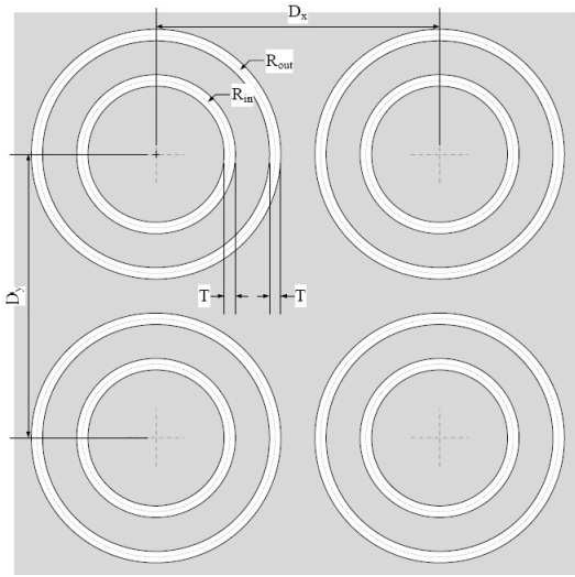

Figure 1. Periodic cell relative to the concentric rings structure.

Table 2. Parameters of the array in Fig. 1.

Parameter	Value
R_{out}	2.5 mm
R_{in}	1.8 mm
T	0.1 mm
D_y	6.1 mm
D_x	6.1 mm

Table 3. Worst computed transmission coefficient S_{21} in band for both polarizations for configuration in Table 2.

Band	S_{21}-TE	S_{21}-TM
Ku Band	−9.1 dB	−9.1 dB
Ka RX Band	−0.3 dB	−0.3 dB
Ka TX Band	−0.1 dB	−0.1 dB

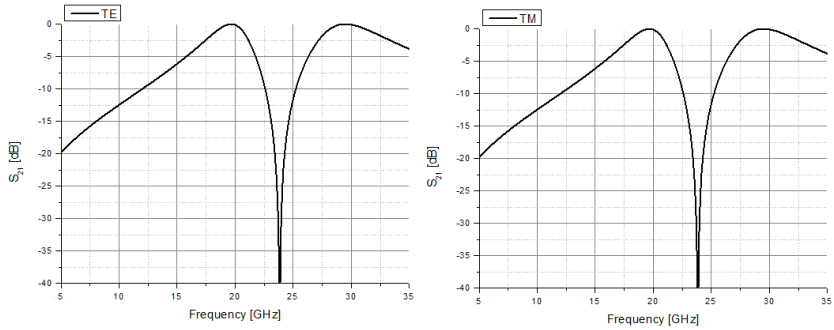

Figure 2. Computed transmission coefficient S_{21} for TE and TM components.

Table 4. Range of frequencies in which the S_{21} is better than -0.5 dB for configuration in Table 2.

Band	Range	BW
Ka RX Band	[19.0–20.5] GHz	1.50 GHz
Ka TX Band	[28.5–31.0] GHz	2.50 GHz

In order to verify the inductive nature of such solution, the surface impedance of the structure in the bands of interest has been simulated. The relative results are shown in Fig. 3. When the curve is near the edge of the circumference, the structure is strongly mismatched with respect to the impedance of the vacuum and consequently a high reflection coefficient occurs. The major part of the energy of the electromagnetic wave is reflected back. The difference of phase between the reflected wave and the incident one can either be positive if the structure presents an inductive surface impedance (upper half of the Smith chart), or negative if the structure presents a capacitive surface impedance (lower half of the Smith chart). It can be seen that in the Ku band the structure is strongly mismatched and presents an inductive surface impedance. On the contrary in both transmission bands (Ka Tx and Rx) the impedance results to be quite well matched. The respective curves are in fact located at the center of the Smith chart. The imaginary part is very close to zero and the real part of the surface impedance is very close to the characteristic impedance of the air (in otherwords, the FSS is almost transparent from the electromagnetic wave point of view).

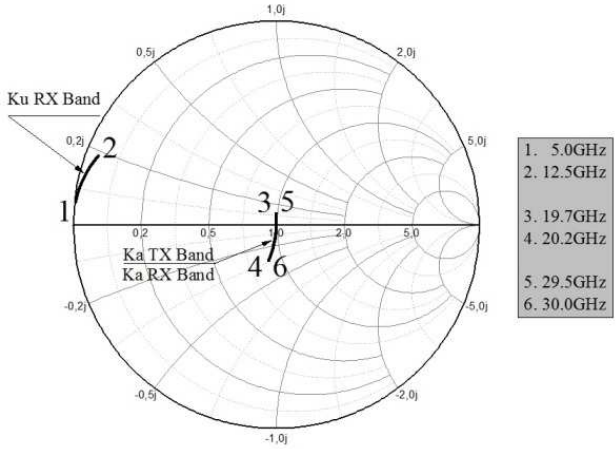

Figure 3. Smith chart of the surface impedance of a FSS with ring apertures on a metallic screen as in Fig. 1.

3.2. Double Ring FSS with Dielectric Substrate

As shown, such a dichroic solution (Design 1) performs quite well but it is not feasable as the two inner metallic rings could not be self-standing. Therefore, in the second design (Design 2), we foresaw the same Double Ring FSS this time placed on a dielectric support made of Teflon with relative permittivity $\varepsilon_r = 2.08$.

It is well known from the open technical literature that increasing the electric permittivity leads to a lower the resonant frequency:

$$2\pi R = \lambda_d = \frac{\lambda_0}{\sqrt{\varepsilon_{eff}}} \tag{2}$$

where ε_r is the effective permittivity defined as [1, 8]:

$$\varepsilon_{eff} = \frac{\varepsilon_1 + \varepsilon_2}{2} = \frac{\varepsilon_r + 1}{2} \tag{3}$$

The presence of a real and an imaginary part of the electric permittivity of Teflon (as given in Fig. 4) modifies the behavior in frequency of the S_{21}. Such a shift towards lower frequencies could be compensated by using smaller elements with respect to those of the first design (see Table 5). Simulation results relative to the re-sized elements are reported in Fig. 5 and in Table 6.

As shown in Table 6, the presence of the dielectric losses leads to additional performance degradation with respect to the performance obtained in the original design (see Table 3). This is clearly true in the Ka sub-bands in which the FSS has been asked to be transparent. The

Table 5. Parameters of the array in Fig. 1 in presence of a dielectric substrate made of Teflon.

Parameter	Value
R_{out}	2.1 mm
R_{in}	1.5 mm
T	0.1 mm
D_y	5.3 mm
D_x	5.3 mm
ε_r	2.08

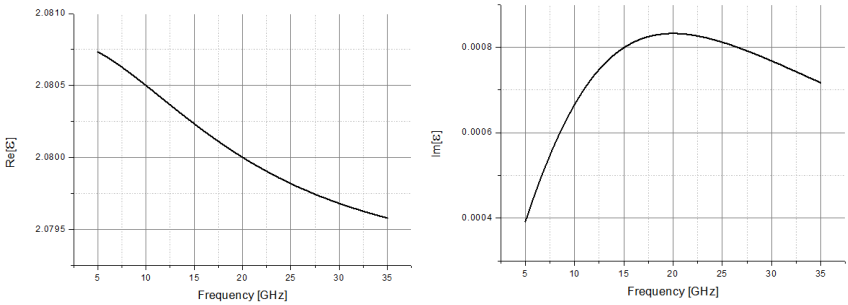

Figure 4. Real and imaginary part of the electric permittivity of Teflon used in simulations.

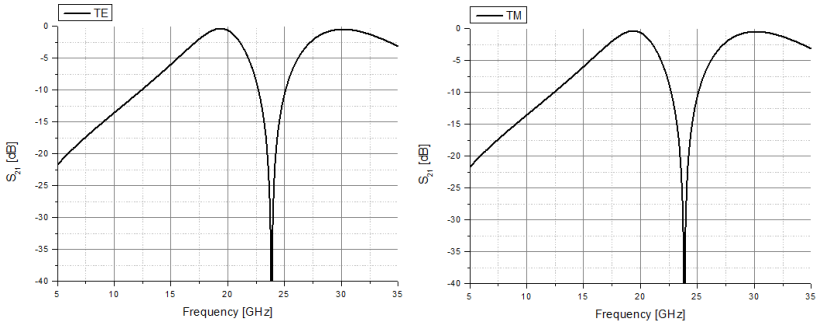

Figure 5. Computed transmission coefficient S_{21} for TE and TM components.

Table 6. Worst computed transmission coefficient S_{21} in band for both polarizations for configuration in Table 5.

Band	S_{21}-TE	S_{21}-TM
Ku Band	−9.4 dB	−9.4 dB
Ka RX Band	−0.9 dB	−1.0 dB
Ka TX Band	−0.6 dB	−0.6 dB

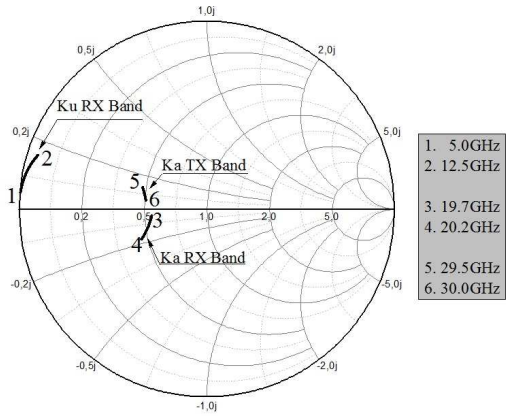

Figure 6. Smith chart of the surface impedance of a FSS with ring apertures on a metallic screen as in Fig. 1 with a dielectric substrate made of Teflon.

surface impedance of the structure in the band of interest is shown in Fig. 6. In Ku band the surface impedance has the same values presented in the previous configuration without dielectric substrate. This is fully in line with the fact that the dielectric substrate was placed in the back of the FSS metal screen (the electromagnetic wave is reflected by the metallic screen that hides the dielectric substrate from the incident wave). On the contrary in the transmitted bands the FSS is almost transparent and the EM wave loses power while passing through the dielectric substrate. As a consequence we can say that the use of FSS employing a periodic array with dielectric substrates should be avoided.

3.3. FSS with Circular Holes

For many reasons, dielectric-free FSS are normally preferable. Therefore a simple thin metal plate perforated with circular-shaped

elements (Fig. 7) has been investigated as third design. This structure is really self-standing as it does not need the presence of any dielectric support.

In this case the radius of the circular hole has been determined at the end of an optimization process. The starting value we used for determining R is given by Eq. (4):

$$R = \frac{c}{2\pi} \frac{x'_0}{f_0} \tag{4}$$

being x'_0 the first zero of the Bessel function $J_1(x)$, c the speed of light in vacuum and $f_0 = 20\,\text{GHz}$ close to the lowest frequency at which we want the FSS to be transparent. Eq. (4) derives directly from the expression of the cut-off frequency of the fundamental mode of a circular waveguide. The thickness of the metallic plate affects the roll-off of the frequency response in the region between the pass and the stop bands.

In Fig. 8, the S_{21} curve of the FSS consisting of circular holes on a metal plate versus frequency is shown. From Table 8, it is clear that this geometry performs well in the reflection band (Ku) and in the lower transmission band (Ka RX band) but has very poor performance in the Ka TX band for both polarizations.

In Fig. 9, the simulated surface impedance is shown on the Smith Chart. In the Ku RX band the surface impedance is strongly inductive and mismatched. It means that the incident wave is almost completely

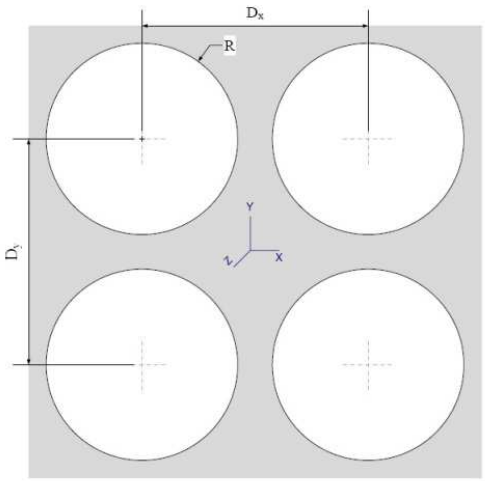

Figure 7. Geometry of the dichroic plate with circular holes.

Table 7. Parameters of the arrays in Fig. 7.

Parameter	Value
R	5.4 mm
D_x	12.3 mm
D_y	12.3 mm

Table 8. Worst computed transmission coefficient S_{21} in band for both polarizations for configuration in Table 7.

Band	S_{21}-TE	S_{21}-TM
Ku Band	−10.1 dB	−10.1 dB
Ka RX Band	−0.1 dB	−0.1 dB
Ka TX Band	−41.5 dB	−41.5 dB

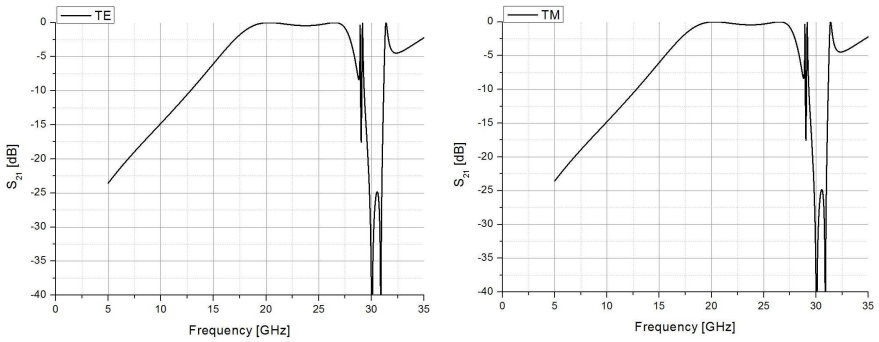

Figure 8. Computed transmission coefficient S_{21} for TE and TM component.

reflected. The same occurs in the Ka TX Band around 30 GHz where the impedance is very far from the matching (center of the Smith Chart) and the structure behaves like a capacitive sheet, therefore its impedance is located on the bottom half of the diagram. In the band around 20 GHz, the FSS is almost transparent for the electromagnetic wave. In fact the scattering parameter S_{21} is about zero in this band (see Fig. 8 and Table 8). To improve the performance in Ka TX band, the designer has not got many degrees of freedom. The only values he might play with are the radius of the circular holes and the

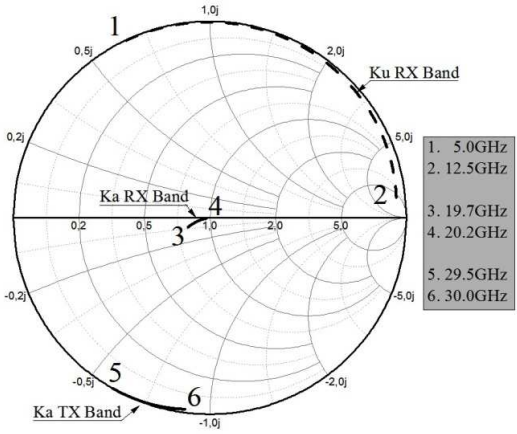

Figure 9. Smith chart of the surface impedance of a FSS with circular holes as in Fig. 7.

thickness of the metallic plate. Unfortunately, each change in one of these two parameters will necessarily affect not only the transmission performance around 30 GHz but also the transmission and reflection performance around 20 and 12 GHz respectively. The performance in one band might be increased at the expenses of performance degradation in one or both other bands. It would be interesting finding a structure able to perform well at 30 GHz without changing the already good results achieved at 12 and 20 GHz. This is achieved in the final design described in Section 4.

4. FSS WITH DOUBLE ALIGNMENT OF DIFFERENT CIRCULAR HOLES

The Double Elements FSS design here proposed can be seen as an enhanced version of the design in Section 3.3 in which we keep the main advantages of the original design (simplicity and absence of dielectric losses) as well as its good electrical performance at Ku-band and Ka RX-bands but we also improve the performance at the Ka TX band by adding/superimposing a second series of holes, generally smaller in size and with arbitrary shape. Doing so, the designer is allowed to play with more degrees of freedom and to find a better compromise between the performance at all the three sub-bands.

In the specific application, we employed this technique to enhance the FSS in Fig. 7 by adding to the original circular holes, smaller holes of exactly the same shape as shown in Fig. 10. This way, it has been

Table 9. Radius of the smaller circular hole of the FSS in Fig. 10.

Parameter	Value
R_2	3.0 mm

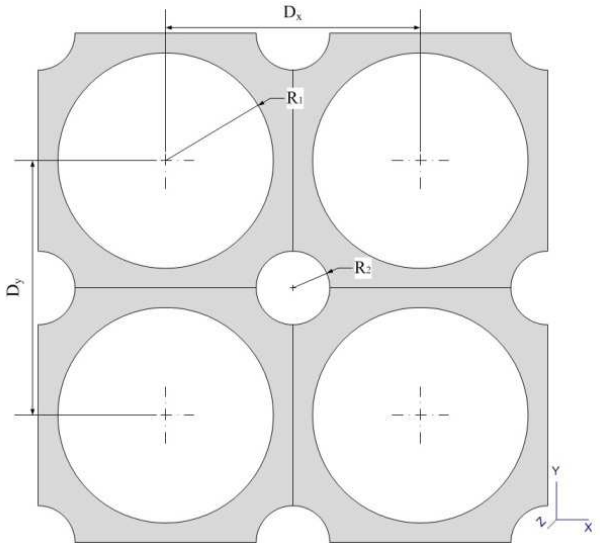

Figure 10. Enhanced inductive FSS with additional smaller circular holes.

possible to adjust the transmission curve locally, i.e., only in a sub-band of interest (in this case the Ka upper band), keeping the rest of the curve essentially unchanged. It is possible to demonstrate that by comparing the results in Section 3.3 with the results in Fig. 11 and in Table 10.

In 2007 Teo [9] and in 2008 Guo [10] proposed two interesting approaches to design a triband FSS, the first in the GPS-GSM1800 bands and the latter around 200 GHz. Nevertheless, in their case one or more dielectric substrates were used and the main limitation is the small band separation. Our solution instead allows to achieve a good transmission behavior in a larger bands separation and the structure does not use any dielectric substrate that leads to the problems already seen in Design 2 (see Section 3.2).

The FSS under analysis has the same geometry dimensions of the circular holes, periodicity and thickness. In Table 9, the 2D dimensions of the circular shaped hole is specified.

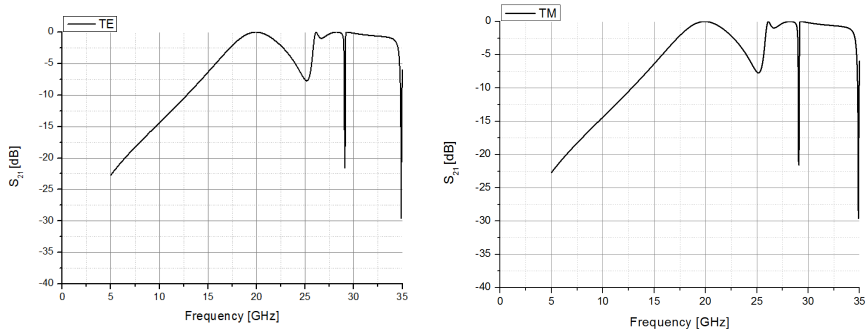

Figure 11. Computed transmission coefficient S_{21} for TE and TM component.

Table 10. Worst computed transmission coefficient S_{21} in band for both polarizations for configuration in Fig. 10.

Band	S_{21}-TE	S_{21}-TM
Ku Band	-10.1 dB	-10.1 dB
Ka RX Band	0 dB	0 dB
Ka TX Band	-0.2 dB	-0.2 dB

Table 11. Ranges of frequencies in which the S_{21} is more than -0.5 dB for configuration in Fig. 10.

Band	Range	BW
Ka RX Band	[18.8–21.1] GHz	2.30 GHz
Ka TX Band	[29.2–31.6] GHz	2.40 GHz

As one can see from Table 10 and Fig. 11, the response for TE and TM excitations are identical as expected for a symmetrical element. In Table 11, the frequency ranges in which the $S_{21} \geq -0.5$ dB are listed. Also in this case, it can be observed that the frequency sub-bands in which the transmission curve has acceptable values are actually wider than those required in specs (Table 1). In Fig. 12, the simulated impedance of the FSS is shown. Comparing it to that of Fig. 9, it can be observed that the impedance in the Ka TX Band is improved in significant way. Now it is very close to the center of the Smith Chart and its values do not change too much within the band. In the

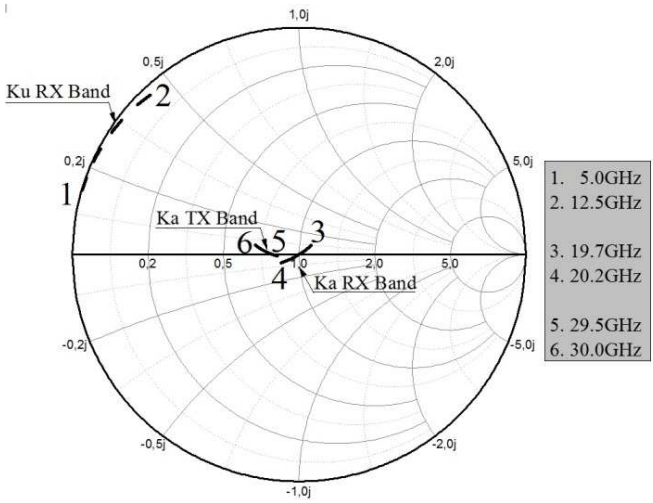

Figure 12. Smith chart of the surface impedance of the structure in Fig. 10.

reflected band till 12 GHz the impedance has a real part very close to zero and a positive imaginary part, so it behaves as an inductor. The overall performances are also comparable to those of an inductive dual-ring FSS in which the size of inner and outer rings are chosen so as to resonate at 20 and 30 GHz (see Section 3.1). The huge advantage of the former FSS with respect to the typical dual-ring FSS is the absence of any dielectric sheet. That makes the proposed design simpler and definitely more attractive because of a significant reduction of the manufacturing costs. Moreover, it is entirely made of metal and it is therefore robust to mechanical stress which may be submitted during its operation on the satellite.

5. CONCLUSION

In this contribution we presented a Dual Elements Inductive FSS Design for Ku/Ka Tri-Band applications. Compared to typical dual ring FSS this solution offers a still well-performing but simpler and cheaper FSS structure. The smaller elements of the two that compose the FSS pattern is chosen so as to refine locally the transmission curve at around higher frequency of interest where typical single hole FSS fail to fulfil the specifications. The strength points of such a solution are the simplicity, the low-cost, the lightweight and the possibility to improve locally the transmission curve of the FSS without affecting

the rest of the curve which already has a satisfactory behavior. The bandwidths of operation of the FSS here proposed are much larger than those required in the specification, but it may be interesting to investigate to expand them even more. This simulated results are very interesting and in the next future a FSS prototype with dual hole pattern will be manufactured and measured.

REFERENCES

1. Munk, B. A., *Frequency Selective Surface: Theory and Design*, Wiley-Interscience, New York, 2000.
2. Munk, B. A., *Finite Arrays and FSS*, Wiley-Interscience, New York, 2003.
3. Schennum, G. H., "Frequency selective surfaces for multiple frequency antennas," *Microwave Journal*, Vol. 16, 55–57, 1973.
4. Huang, J., T. Wu, and S. Lee, "Tri-band FSS with circular ring elements," *IEEE Trans. Antennas Propagation*, Vol. 42, No. 2, 166–175, 1994.
5. Wu, T. K. and S. Lee, "Multiband frequency selective surface with multiring patch elements," *IEEE Trans. Antennas Propagation*, Vol. 42, No. 11, 1484–1490, 1994.
6. Wu, T. K., "Single screen triband FSS with double square loop elements," *Microwave and Optical Tech. Lett.*, Vol. 5, No. 2, 56–59, 1992.
7. Luol, X. F., P. T. Teo, A. Qing, and C. K. Lee, "Design of double square loop frequency selective surfaces using differential evolution strategy coupled with equivalent circuit model," *Microwave and Optical Tech. Lett.*, Vol. 44, No. 2, 94–97, 2005.
8. Orfanidis, S. J., *Electromagnetic Waves and Antennas*, Rutgers University, 2008.
9. Teo, P. T., X. F., Luo, and C. K. Lee, "Frequency selective surfaces for GPS and DCS 1800 mobile communication, Part 1: Quad-layer and single-layer FSS desig," *IET Microw. Antennas Propag.*, Vol. 1, 314–321, 2007.
10. Guo, C., H. Sun, and X. Lu, "A novel dualband frequency selective surfaces with periodic cell perturbation," *Progress In Electromagnetics Research B*, Vol. 9, 137–149, 2008.